Large-Scale Modeling Approach Reveals Functional Metabolic Shifts during Hepatic Differentiation

Nathalie Poupin, Anne Corlu, Nicolas J. Cabaton, Hélène Dubois-Pot-Schneider, Cécile Canlet, Elodie Person, Sandrine S. Bruel, Clément Frainay, Florence Vinson, Florence Maurier, et al.

A large-scale modelling approach reveals functional metabolic shifts during hepatic differentiation

Nathalie Poupin[*1], Anne Corlu[2], Nicolas J. Cabaton[1], Hélène Dubois-Pot-Schneider[2]†, Cécile Canlet[1], Elodie Person[1], Sandrine Bruel[1], Clément Frainay[1], Florence Vinson[1], Florence Maurier[1]‡, Fabrice Morel[2], Marie-Anne Robin[2], Bernard Fromenty[2], Daniel Zalko[1] and Fabien Jourdan[1]*

[1]UMR1331 Toxalim (Research Centre in Food Toxicology), Université de Toulouse, INRA, ENVT, INP-Purpan, UPS, Toulouse, France

[2]Univ Rennes, INSERM, INRA, Institut NUMECAN (Nutrition Metabolisms and Cancer) UMR_A 1341, UMR_S 1241, F-35000 Rennes, France

Corresponding Author

*E-mail: nathalie.poupin@inra.fr

ABSTRACT

Being able to explore the metabolism of broad metabolizing cells is of critical importance in many research fields. This article presents an original modelling solution combining metabolic network and omics data to identify modulated metabolic pathways and changes in metabolic functions occurring during differentiation of a human hepatic cell line (HepaRG). Our results confirm the activation of hepato-specific functionalities and newly evidence modulation of other metabolic pathways, which could not be evidenced from transcriptomic data alone. Our method takes advantage of the network structure to detect changes in metabolic pathways that do not have gene annotations, and exploits flux analyses techniques to identify activated metabolic functions. Compared to usual cell-specific metabolic network reconstruction approaches, it limits false predictions by considering several possible network configurations to represent one phenotype, rather than one arbitrarily selected network. Our approach significantly enhances the comprehensive and functional assessment of cell metabolism, opening further perspectives to investigate metabolic shifts occurring within various biological contexts.

KEYWORDS: Genome scale metabolic modelling / global metabolic shifts / HepaRG cell line / hepatic differentiation / transcriptomics and metabolomics

INTRODUCTION

Getting a global picture of how cell metabolism is reprogrammed or shifted under different conditions is a crucial step towards the understanding of how cellular metabolic functionalities can be altered or modified under the induction of internal processes (*e.g.,* cell differentiation) or external factors (*e.g.,* toxics or drugs). Technological advances in high-throughput DNA and RNA sequencing methods now enable the analysis of the complete genome or transcriptome of a given cell or organism, providing a first large-scale picture of its biological status under a given condition. However, this information is often not sufficient to describe nor predict the metabolic phenotype of the studied system, as metabolic processes involve many interconnected reactions, whose final resulting activities are not always directly and strictly related to the observed gene expression levels. Understanding the metabolic behavior of cells and tissues in given conditions requires apprehending this complex network of reactions at the whole genome scale.

In this perspective, genome-scale metabolic network reconstructions (GSMNR) open promising possibilities for shaping a comprehensive picture of the metabolism and its modulation within various contexts, such as development, pathological processes, or under drug exposure. These reconstructions aim at assembling all the biochemical transformations known to occur in a given organism, based on its genome annotation and data available from the literature [1]. They include information about the gene-protein-reactions (GPR) associations, which describe the relationships between the metabolic reactions, the enzymes that catalyze them, and the genes these enzymes are encoded by. Hence, GSMNR provide a relevant scaffold for the mechanistic analysis and interpretation of gene expression profiles in terms of metabolic phenotype. To date, several generic reconstructions have been published for the human metabolic network (Recon 1 [2]; EHMN [3]; HMR2 [4]; Recon 2 [5]; Recon2.1 [6]; Recon 2.2 [7]; iHsa [8]; Recon 3D [9]). These reconstructions represent the overall theoretical metabolic capacity of a generic human cell or tissue, regardless of external

conditions or cell or tissue specificities, and encompass up to 13000 reactions and 3700 genes for the latest reconstruction. Because of their genericity, these reconstructions cannot directly be used to predict accurately cell- or tissue- specific metabolic behaviors. They need to be tailored to more specific subnetworks, by identifying the reactions from the original generic GSMNR that are specifically active in the studied cell, tissue or conditions. Several methods have been proposed to tackle this challenge and have already succeeded in capturing the specific metabolic features of tissues [10–12] or cancer cells [13–17]. These methods use experimental data (*e.g.,* transcriptomic or proteomic data) to predict a consistent subnetwork of reactions specifically active in the studied condition that best matches with the experimental data. The algorithms used for this purpose rely on constraint-based modeling (CBM) approaches, which aim at calculating the steady-state fluxes of metabolites, *i.e.,* the rates of metabolic conversion or transfer, through each network reaction [18].

In this study, we propose a generic approach, based on the human GSMNR Recon 2, and on transcriptomic and metabolomic data, to identify global changes in metabolic functions between two cell populations. We based our new method on a previously published algorithm for tissue-specific network reconstruction, the iMat algorithm [10,19], with the originality that we depicted the metabolism of the each cell population by a set of subnetworks rather than one unique subnetwork. We hypothesize that this approach enables to better characterize the whole metabolic capability of a cellular system independently of specific conditions and limits the risk of false predictions. We applied this approach for comparing the metabolism of the human hepatic cells HepaRG in two distinct differentiation stages: undifferentiated progenitor cells and fully differentiated hepatocyte-like cells. The HepaRG cell line, which is derived from a human hepatocellular carcinoma, is a relevant human model to study hepatic cell differentiation, as it has the particularity to exhibit features of bipotent progenitor cells but is also able to differentiate into mature hepatocyte-like cells. These fully differentiated hepatocyte-HepaRG cells have been demonstrated to display

metabolic capacities close to primary human hepatocytes, and in particular, to express numerous xenobiotic metabolizing enzymes [20,21] and to present functional mitochondria [22]. Hepatic cell differentiation is a key process in liver maintenance and regeneration and many liver diseases may imply, to some extent, hepatic regenerative processes. Therefore, being able to compare the metabolic capabilities of cells at different developmental stages in *in vitro* models is a critical step when aiming to generate fully functional hepatocytes for liver transplantation or to study disease or toxicological mechanisms [23]. Metabolic differences between pluripotent stem cells and differentiated cells have been reported [24–26], but studies providing a more global overview of the metabolic shifts occurring during re-programming and differentiation are still lacking. Besides, most studies investigating the differences between progenitors and differentiated HepaRG cells have so far focused on a set of selected transcripts or proteins associated with the expression of enzymes involved in xenobiotics metabolism or with liver-specific functions (such as albumin production) [20,27,28]. A few global methylomic or transcriptomic analyses have enabled to further explore the modulations occurring at the regulation level upon differentiation and have reported the modulation of global cellular processes (such as cell cycle, cell death, apoptosis, cell morphology …) [29,30]. However, information is still missing about the modulations occurring at the metabolic level and involving sustainable changes in metabolic capacities and functionality of these cells. The global approach we propose in this study intends to help generating a global picture of the metabolism of HepaRG cells. In comparison to usual transcriptomic analyses, the method we developed takes advantage of the network structure to go beyond the descriptive analysis based on metabolic pathways and to gain information about the functional capacity of the cells, without focusing on one *a priori* defined restricted set of metabolic features or genes.

MATERIALS & METHODS

HepaRG cell culture

The HepaRG cells, kindly given by Dr C. Guguen-Guillouzo, were cultured according to the standard protocol described by Aninat et al. [20]. Briefly, HepaRG cells were seeded at a density of 2.4x104 cells/cm² in a growth medium composed of William's E medium (Gibco, Illkirch, France) supplemented with 10% fetal bovine serum (HyClone, Thermo Scientific, Illkirch, France), 100 U/ml penicillin and 100µg/mL streptomycin, 5 µg/mL insulin, 2mM glutamine (Sigma, Saint-Quentin Fallavier, France) and 50 µM hydrocortisone (Serb, Paris, France). Undifferentiated HepaRG cells were collected after 3 days of culture on this medium ("3-day cells"). To obtain differentiated HepaRG cells, cells were cultured in the initial medium for 2 weeks, then switched to a medium supplemented with 2% DMSO (Sigma) and cultured on this supplemented medium for 2 more weeks. Addition of DMSO induces of HepaRG cells to two different cell types: hepatocyte-like cells and biliary like-cells. HepaRG cells corresponding to fully differentiated hepatocytes were called "30-day cells".

Microarray analyses

Total messenger RNA (mRNA) from four biological replicates was extracted from 3-day and 30-day HepaRG cells. mRNA was checked for purity and integrity, using an Agilent Bioanalyser (Agilent Technologies, Palo Alto, CA). Genome-wide expression profiling was performed using the low-input QuickAmp labeling kit and human SurePrint G3 8x60K pangenomic microarrays (Agilent Technologies, Santa Clara, CA, USA). Gene expression data were processed using Feature Extraction and GeneSpring software (Agilent Technologies).

Genes were classified in 2 categories according to their expression level. Genes whose expression level was below the defined threshold of 150 were considered as not detected or not expressed (NE), whereas genes whose expression level was above 150 for all replicates were considered as

significantly expressed (HE). In addition, genes that were found to be significantly up-regulated between d3 and d30 (p-value <0.01 with an unpaired t-test adjusted with Bonferoni correction and with a fold change higher than 2) were considered as significantly expressed (HE) at d30 and, similarly, down-regulated genes were considered as significantly expressed at d3. The threshold value of 150 corresponds as the 25 percentile of the gene expression level among all genes and all replicates, which is generally considered as the background noise in Agilent microarray experiments.

Metabolomic analyses

Metabolites were extracted from 1 million of cells with an acetonitrile/water (1:9) solvent mixture. Samples were centrifuged 10 minutes at 5000 g. Supernatants were evaporated using a SpeedVac and resuspended in deuterated water (D20), samples were vortexed and transferred into 5 mm NMR tubes.

1H NMR spectra of cell extracts were acquired on a Bruker Avance spectrometer (Bruker, Karlsruhe, Germany) operating at 600.13 MHz, and equipped with an inverse detection 5 mm TXI 1H-13C-15N cryoprobe connected to a cryoplatform. Spectra were acquired using a Carr-Purcell-Meiboom-Gill (CPMG) spin echo pulse sequence with a 2 seconds relaxation delay to attenuate macromolecules signals. A water suppression signal was achieved by presaturation during the relaxation delay. The spectral width was set to 20 ppm for each spectrum and 512 scans were collected with 32K points. Free induction decays were multiplied by an exponential window function before Fourier Transformation. The spectra were manually phased and the baseline was corrected using TopSpin 3.2 software (Bruker, Karlsruhe, Germany).

Metabolites were identified using the literature, home-made and freeware databases such as the Human Metabolome Database ([31]; www.hmdb.ca/).

Implementation and adaptation of the iMat algorithm to generate stage-specific metabolic models of HepaRG cells

We used the generic human metabolic network reconstruction Recon 2 ([5]; version 2.04, downloaded from http://vmh.uni.lu/#downloadview) as a framework for the prediction of active metabolic reactions in the HepaRG cells. This genome-scale metabolic network reconstruction encompasses 7440 reactions, 2140 genes and 2626 unique metabolites and is supposed to represent the comprehensive metabolic capacity of any human cell or tissue. The network reconstruction is converted into a mathematical model, where the list of metabolic reactions is described as a stoichiometric matrix (S). This matrix defines which metabolites (enumerated as rows) participate in each of the network reactions (enumerated as columns), with numerical entries in the matrix representing the stoichiometric coefficients of the reactions.

First, gene expression data were mapped to the network reactions by using the Gene-Protein-Reaction (GPR) association rules defined in the network reconstruction. We used these GPR associations to determine a set of a priori highly expressed reactions (HEr) or not expressed reactions (NEr) according to the expression level of their associated gene(s). In the case of "AND" GPR associations, we classified the reaction as HEr (or NEr respectively) if all genes were HE (or NE respectively), whereas in the case of "OR" associations, the reaction was considered as HEr if any of the associated gene was HE. In the initial Recon 2 reconstruction, 4821 reactions had defined GPR associations.

We then implemented the iMat algorithm [10], that we adapted, in order to predict which reactions from the generic metabolic network Recon 2 were specifically active in the HepaRG cells (Figure S1). As initially proposed by Shlomi et al., the optimization problem was formulated as a Mixed Integer Linear Programming (MILP) problem, to find a steady-state flux distribution that maximizes the number of reactions whose flux is consistent with the measured expression level of

their associated gene(s) and that complies with stoichiometric and thermodynamic constraints. In our modified version of this algorithm, we added some constraints so that the predicted flux distribution is also in agreement with the metabolomics data, meaning that it allows all detected metabolites to be produced. More precisely, for each identified metabolite, at least one reaction that is able to produce it in the model should have a non-zero flux.

max $\sum_{i \in HE_r}(y_i^+ + y_i^-) + \sum_{i \in NE_r} y_i$

ν, y^+, y^-, y

subject to

$$S.\,\nu = 0 \quad (1)$$

$$\nu_{min} \leq \nu \leq \nu_{max} \quad (2)$$

$$\nu_i + y_i^+ (\nu_{min,i} - \varepsilon) \geq \nu_{min,i}\ ,\ i \in HEr \quad (3)$$

$$\nu_i + y_i^- (\nu_{max,i} + \varepsilon) \leq \nu_{max,i}\ ,\ i \in HEr \quad (4)$$

$$\nu_i + y_i \cdot \nu_{min,i} \geq \nu_{min,i}\ ,\ i \in NEr \quad (5)$$

$$\nu_i + y_i \cdot \nu_{max,i} \leq \nu_{max,i}\ ,\ i \in NEr \quad (6)$$

$$\nu_{i(j)} + x_{i(j)}^+ (\nu_{min,i(j)} - \varepsilon) \geq \nu_{min,i(j)}\ ,\ \text{for } (j \in \text{obs. mets}) \,\&\, (i \in RProd_j) \quad (7)$$

$$\nu_{i(j)} + x_{i(j)}^- (\nu_{max,i(j)} + \varepsilon) \leq \nu_{max,i(j)}\ ,\ \text{for } (j \in \text{obs. mets}) \,\&\, (i \in RProd_j) \quad (8)$$

$$\sum_i x_{i(j)} \geq 1,\ \text{for } [j \in ExpMets] \quad (9)$$

$$y_i^+,\ y_i^-,\ y_i,\ x_i^+,\ x_i^- \in [0;1]$$

ν is the flux vector and S is the stoichiometric matrix.

Equation (1) ensures that flux values comply with the mass balance constraints. Thermodynamic and capacity constraints are imposed by equation (2): restricted direction and values for reaction flux, according to these constraints, are defined in ν_{min} and ν_{max} vectors (minimal and maximal flux

values respectively), which are set as lower and upper bound for reaction flux values. Equations (3) to (6) set constraints corresponding to gene expression data. y_i^+, y_i^- and y_i are boolean variables representing the adequacy between the predicted flux v_i through reaction i and its expression level. For HEr, y_i^+ (y_i^-) represents whether the reaction is active in the forward (or backward, respectively) direction: equations (3) & (4) enforce that, if $y_i^+=1$ or $y_i^-=1$ (*i.e.,* the reaction is active), the value of the flux through reaction i is larger than a threshold ε, whereas if $y_i^+=0$ or $y_i^-=0$ (*i.e.,* the reaction is inactive), the flux through reaction i must be 0. For NEr, y_i represents whether the reaction is inactive: equations (5) & (6) enforce that, if $y_i=1$ (*i.e.,* the reaction is inactive), the flux through reaction i is 0. A threshold of 0.1 was used to predict the activity of reactions. Different threshold values were tested and provided qualitatively similar results. Equations (7) to (9) set constraints corresponding to metabolomic data. For each identified metabolite j ("ExpMets"), "$RProd_j$" encompass all reactions i that can produce this metabolite according to the stoichiometric matrix S. x_i^+ (or x_i^-, respectively) are Boolean variable representing whether the reaction i is active or not in the forward (or backward, respectively) direction. When $x_i^+ = 1$, the flux through reaction i must be larger (or smaller, respectively) than ε (equation (7)), forcing the reaction to be forward active. For reversible reactions, when $x_i^- = 1$, the flux through reaction i must be negative and lower than ε (equation (8)), forcing the reaction to be backward active. If $x_i^+=0$ and $x_i^-=0$, the flux through reaction i is forced to be 0, forcing the reaction to be inactive. The constraints set in Eq. 9 ensure that at least one reaction is able to produce the metabolite j is active.

The optimization problem consists in finding the flux distribution v, which maximizes the number of HEr which are active ($v_{HEr} \geq \varepsilon$) and the number of NEr which are inactive ($v_{NEr} = 0$). This sum represents the "adequacy score" of the flux distribution. The percentage of adequacy is calculated as the adequacy score divided by the theoretical maximal adequacy score that could be

obtained (*i.e.*, the sum of all reactions associated with HE genes and the sum of all reactions associated to NE genes).

The algorithm was implemented in Matlab 2014a (The Mathworks, Natick, MA, USA) and the resolution of the MILP problem was performed using the ilog CPLEX solver version 12.6.0 (ILOG, Sunnyvale, CA, USA).

Identification of alternative adequate stage-specific subnetworks equally fitting the experimental data

The flux distribution obtained by solving the MILP problem is optimal in term of adequacy with transcriptomic and metabolomic data, but is not unique. Alternative solutions exist that have the same adequacy with experimental data. To explore the space of alternative solutions, as proposed by Shlomi *et al*. and in a further study [32], we searched whether, for each reaction that was predicted to be active (or inactive, respectively) in the first optimal solution, a solution with a similar adequacy score could be found with this reaction being inactive (or active, respectively) (Figure S1C). From the initial computed flux distribution, each reaction was successively forced to be either active (*i.e.,* to carry a non-zero flux, with $\nu \geq \varepsilon$) or inactive ($\nu = 0$) and a new MILP optimization was performed. Reversible reactions were successively set to be active in each direction ($\nu \geq \varepsilon$, then $\nu \leq -\varepsilon$). Only flux distributions having a maximal adequacy score were kept, forming the final set of optimal solutions. Each of these solutions represents a subnetwork of predicted active reactions, with optimal adequacy with experimental data. The same computations were performed independently using the data obtained at d3 and d30, providing one set of equally adequate subnetworks with regard to gene expression data for each d3 and d30 stage.

For each stage, reactions that were found to be active in all possible subnetworks were considered as "required" (R) reactions, meaning that no maximal adequacy score could be achieved when these reactions were forced to be inactive. Conversely, reactions that display a zero-flux in all the optimal

solutions were considered as "Inactive" (I) reactions, since no maximal adequacy score could be achieved when these reactions were forced to be active. All other reactions that are either active or inactive in the optimal solutions were considered as "Potentially active" (PA) reactions. As a result, sets of R, PA and I reactions were defined for each stage (Figure S1D).

Assessment of the liver-specificity of genes in generated subnetworks

To evaluate the liver-specificity of our generated models, we assessed, for each subnetwork, the number of predicted "expressed" genes that can be considered as liver-specific. We used information about the tissue location of genes from the UNIPROT [33] and the Human Protein Atlas (HPA[34]) databases.

First, for each generated subnetwork, genes predicted as "expressed" were inferred from the predicted active reactions using the GPR rules. UNIPROT identifiers for Recon 2 genes were retrieved from their EntrezGene identifiers (as available in the initial reconstruction) using the DAVID database [35] and predicted "expressed" genes were compared to genes with evidence for presence in the liver according to the UNIPROT database. For each subnetwork, we calculated the "recall" of liver-specific genes, as the proportion of Recon 2 genes with evidence of presence in liver that were predicted to be "expressed" in the subnetwork, and the "precision", as the proportion of predicted "active" genes in the subnetwork that were liver located.

In a second analysis, we mapped the confidence level for protein expression in liver hepatocytes assigned in the HPA database (High, Medium, Low or Not detected) to the generated subnetworks and evaluated, in our HepaRG 3-day and 30-day subnetworks, the proportion of predicted active reactions associated with high, medium or low confidence level for protein expression in liver according to the HPA database. The recall of reactions associated with high confidence for liver expression was calculated as the proportion of reactions with high confidence level that were

predicted to be active in each subnetwork. The precision was calculated as the proportion of predicted active reactions that had a high confidence level.

Simulation of achievable metabolic functions in generated subnetworks

We performed flux balance analysis to test whether our generated subnetworks were able to achieve some defined metabolic functions. A list of 155 metabolic functions (SI Table S1), including 111 generic functions (*i.e.,* functions assumed to be fulfilled by any tissue or cell independently of its type) and 44 hepato-specific functions, was gathered from previous publications [4,36,37]. For each of these tasks, we defined a corresponding objective function and maximized it to check whether it could carry a non-zero flux. The sets of metabolites that could be taken up and released was restrained to mimic a minimal standard medium and adjusted depending on the specific metabolic objective tested. For instance, we tested the ability of our models to perform gluconeogenesis (the formation of glucose from various gluconeogenic substrates) by restraining the set of metabolites that could be taken up to only non-carbon sources (O_2) except for lactate and glucogenic amino acids (alanine, glutamine …) and maximize the excretion of glucose. This functional testing was performed for each of the generated subnetworks at both d3 and d30. We verified that all the 155 defined metabolic functions could be achieved by the initial Recon 2 model. The complete list of tested metabolic functions and corresponding applied constraints for uptake and secretion is provided in supplemental Table 1.

Analysis of the variability among generated subnetworks

PCA was performed on all generated subnetworks, independently of the stage. Reactions were used as variables and each subnetwork was represented by a vector of binary values corresponding to the predicted activity state of each reaction (0 for predicted inactive reactions and 1 for predicted active reactions).

Pathway enrichment analyses for identification of activated and inactivated pathways

Reactions were considered as inactivated during the differentiation if they were predicted to be active in at least one subnetwork (R or PA) at d3 and inactive at d30, and conversely activated if they were predicted to be inactive at d3 and R or PA at d30. Pathway enrichment analyses were performed over activated and inactivated reactions to assess whether the given reactions were significantly over-represented in a metabolic pathway. Pathway enrichment statistics were performed using one-tailed exact Fisher test, with a Bonferroni correction for multiple tests [38], using the metabolic pathways defined in Recon 2.04. Blocked reactions, identified using flux variability analysis, were excluded from the background set of Recon 2 reactions. Pathway enrichment analyses were also performed for the sets of highly or not expressed genes.

Assessing the benefits of the developed approach: comparison with predictions made from transcriptomic data only

To assess the interest of using the network topology and stoichiometry to predict the metabolic modulations occurring during the differentiation process, we performed pathway enrichment analyses on genes identified as up or downregulated between the two stages. Genes were considered as upregulated if they were classified as NE at d3 and HE at d30 and inversely, downregulated, if they were classified as HE at d3 and NE at d30.

Assessing the benefits of the developed approach: comparison with predictions made from single solutions

We compared our predictions with predictions that would be obtained when considering only one individual optimal subnetwork instead of a set of optimally adequate subnetworks for each stage. For each stage, we selected two distinct individual solutions “iMat-A” and “iMat-B” among all the equally adequate generated subnetworks. "iMat-A" is the first initial optimal solution, corresponding to the one returned by the iMat algorithm such as implemented in the CobraToolbox. “iMat-B” is one other randomly selected solution among all optimal solutions. We also compared

our results with results obtained by using the FASTCORE algorithm [39], which provides with one particular solution minimizing the number of active reactions ("FASTCORE solution"). For each stage, we used the set of reactions associated with highly expressed genes as input for the "core reactions set" in the FASTCORE algorithm, which then returns a minimal flux consistent subnetwork containing all the reactions from this core set and a minimal set of additional reactions. To compare individual solutions to the whole set of subnetworks, we considered the union of subnetworks. For liver-specific genes, we considered all the genes that were predicted to be expressed in any of the cell-specific subnetworks. For reactions predicted to be activated in the union of equally adequate subnetworks, we considered all the reactions that were predicted to be active in any of the 30-day cell-specific subnetworks but inactive in all 3-day cell-specific subnetworks. Inversely for reactions predicted to be inactivated in the union of subnetworks, we considered all the reactions that were predicted to be inactive in any of the 30-day subnetworks but active in all 3-day subnetworks.

Data availability

Gene expression data have been deposited in the Gene Expression Omnibus (GEO) database under the accession number GSE112123. NMR metabolomic data are provided as Supporting Information (Table S2).

RESULTS

In this study, we aimed at comparing the differences in metabolic functions expressed in 3-day (non-differentiated) progenitor HepaRG cells ("3-day cells") *vs.* 30-day fully differentiated hepatocyte-like HepaRG cells ("30-day cells"), using a large-scale modelling approach. To that purpose, we defined consistent metabolic models that distinctively represent the functional metabolism of 3-day cells and 30-day cells. We used the generic genome scale metabolic reconstruction Recon 2 [5] as a scaffold to integrate transcriptomic and metabolomic data and predicted which of the Recon 2 reactions would be specifically active or inactive at each differentiation stage in HepaRG cells. Prediction of the reaction activities was computed using the iMat algorithm proposed by Shlomi *et al.* [10] that we adapted to fit the specific objectives of our study. Figure S2 illustrates the pipeline followed in this study.

Experimental transcriptomic and metabolomic data provide only partial coverage of the metabolic network

For each differentiation stage, we identified expressed (HE) or not expressed (NE) genes from the experimental data set and transferred this information to reactions using the GPR associations. As expected, only a small proportion (9%) of the genes classified as HE or NE from the experimental data set could be mapped into Recon 2, these mapped genes representing 32% of the metabolic genes currently annotated in Recon 2 (Figure S3A&B). According to GPR associations, 29-31% of Recon 2 reactions could be linked to gene expression data (Figure S3C). More precisely, 16% and 21% of Recon 2 reactions were associated with HE genes at day 3 (d3) and day 30 (d30), respectively, whereas 13% (d3) and 10% (d30) were associated with NE genes. Of note, the relation between reactions and genes is not bijective: one reaction can be linked to several distinct genes, for instance when several isoenzymes are involved, and conversely one gene product can control more than one reaction. For instance, for the carnitine palmitoyltransferase 1A gene (CPT1A,

hsa:1374), the encoded protein can catalyze the transfer of the acyl group of different long-chain fatty acids (FAs) onto carnitine. In parallel, NMR analyses allowed the detection and identification of 36 and 34 metabolites in 3-day and 30-day HepaRG cells, respectively, out of which 34 (d3) and 32 (d30) metabolites could be mapped into Recon 2 (Table S2).

Reconstruction of stage-specific cell models from experimental data: multiple possible subnetworks for 3-day and 30-day cells

The cell-specific metabolic network reconstruction algorithm uses gene expression levels as clues to predict the activity state of the associated reactions. It relies on CBM methods to find metabolic flux distributions, which (1) maximize the number of reactions whose predicted flux is consistent with associated gene expression level and (2) comply with the stoichiometric constraints imposed by the network topology. We adapted the iMat algorithm so that the predicted flux distributions would also take into account metabolomics data (see Material and Methods).

We identified several flux distributions having a similar adequacy with the experimental gene expression data, as assessed by the "adequacy score" (*i.e.*, the proportion of reactions whose predicted activity state is in adequacy with the transcriptomic data). One predicted flux distribution corresponds to a set of active reactions (*i.e.*, reactions carrying a non-zero flux) representing a consistent and fully connected subnetwork. We identified 3534 distinct subnetworks having a maximal adequacy score of 75% for the 3-day cells, and 3313 distinct subnetworks with an adequacy score of 72% for the 30-day cells (Table S3). These two sets of equally optimal subnetworks will be subsequently referred to as "cell-specific models". As imposed by the modeling constraints, all distributions enable the production of the set of NMR identified metabolites. We tested that no better adequacy with transcriptomic data could be obtained when releasing the additional constraints imposed from metabolomic data (see Material & Methods for

details), which means that there was no specific disagreement between transcriptomic and metabolomic data. The number of predicted active reactions was significantly higher in 30-day cell-specific models than in 3-day cell-specific models, ranging from 2842 to 3036 at d30 (median: 2931) and from 2445 to 2673 (median: 2567) at d3 (Figure S4). The predictions of reactions activity for all subnetworks are provided in Table S4.

Rather than selecting only one arbitrary subnetwork, we chose to take into account all the alternative solutions we found to be equally adequate with the experimental data for each differentiation stage. Reactions that were consistently predicted to be active in all subnetworks for one differentiation stage were considered as "required reactions" (R) whereas reactions whose predicted activity varied across subnetworks were considered as "potentially active" (PA) (Figure S2B). 56% and 60% of Recon 2 reactions were globally predicted to be active, either PA or R (*i.e.*, active in at least one subnetwork), at d3 and at d30 respectively. At d30, 37% of these active reactions were predicted to be required, whereas a slightly lower proportion of R reactions was found at d3 (27%) (Figure 1A). We identified two main causes contributing to the high number of alternative possible subnetworks. The first one is the lack of gene expression information for some reactions. Globally, we observed that reactions with a variable predicted activity state (PA reactions) are associated with gene expression data in a higher proportion (2%) than reactions with consistent predicted activity among stage-specific models (R reactions; 58%). The second one is the existence of several alternative reactions performing the same metabolic transformation. For instance, some biochemical conversions happen to be described by two alternative paths that use a different number of reaction steps or the same reactions are sometimes duplicated with more than one tissue-specific annotation. As a striking example, in the N-glycan synthesis pathway of the Recon 2 network, two alternative paths of 22 reactions enable the synthesis of the glycan precursor before it is bound to a protein in the endoplasmic reticulum (ER) and further processed in the ER

and Golgi apparatus. The two paths only differ by the fact that the reactions are annotated as liver reactions ("_L") in one and as uterine reactions ("_U") in the other. These 44 reactions have been identified through Principal Component Analysis (PCA) as the reactions that contribute the most to the discrimination between subnetworks within each set of stage-specific subnetworks (Figure S5) demonstrating that path redundancy can contribute to the variability among subnetworks.

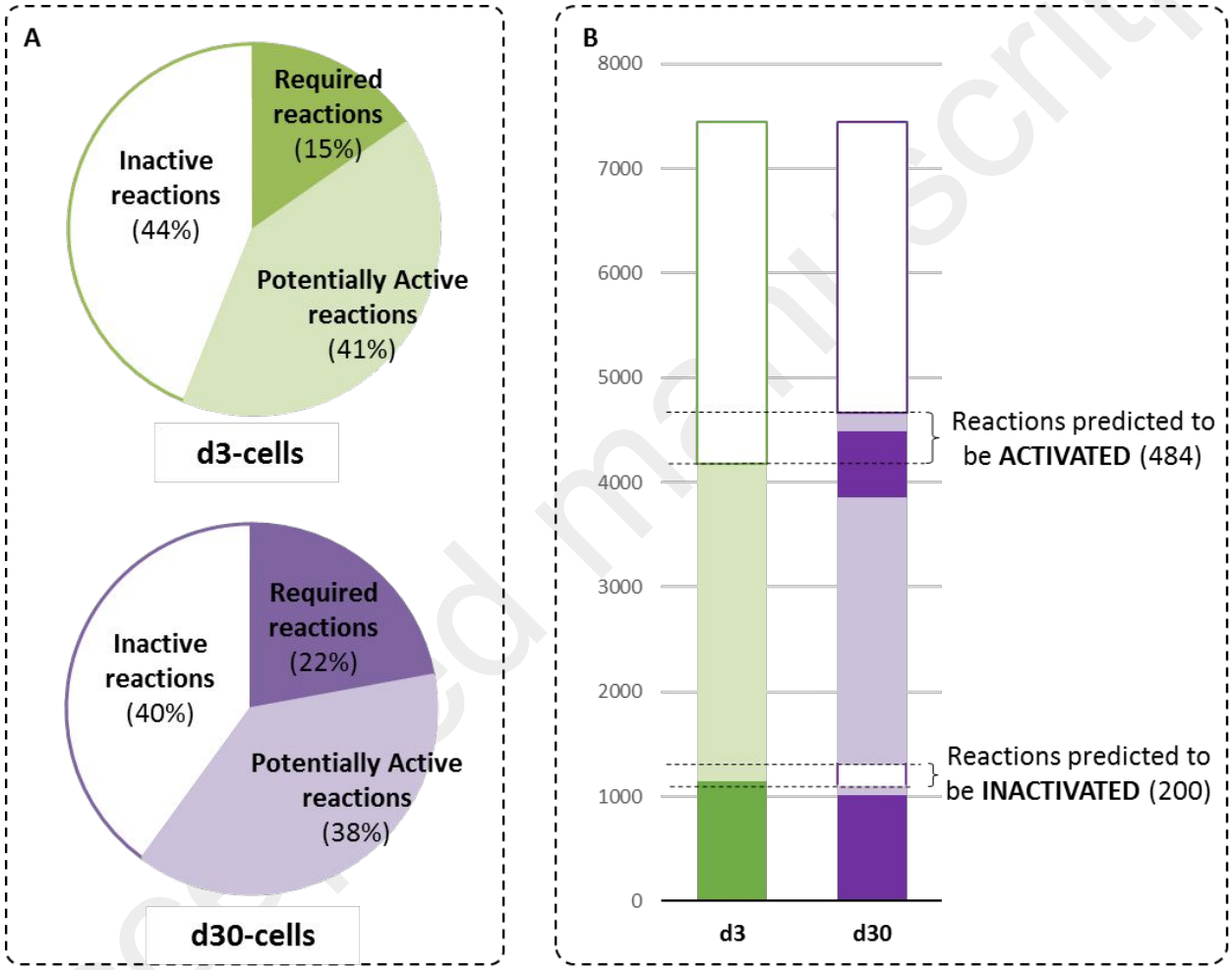

Figure 1. Predicted activity of Recon 2 reactions in stage-specific subnetworks.

Comparison of stage-specific subnetworks: evidences for global metabolic changes during the differentiation process

To investigate which significant metabolic changes occur between 3-day and 30-day HepaRG cells, we compared the cell-specific models generated for each stage. We first performed an unsupervised discriminant analysis (PCA) of all the cell-specific models together. The score plot of the PCA analysis showed a clear separation between the two stages, with more than 40% of the variability explained by the differentiation stage represented along the first axis (Figure 2). This demonstrates not only that there are metabolic differences between these two stages, but also that these differences exceed the differences between the subnetworks within each stage, which is represented by the second axis and accounts for only 2.5% of the total variability.

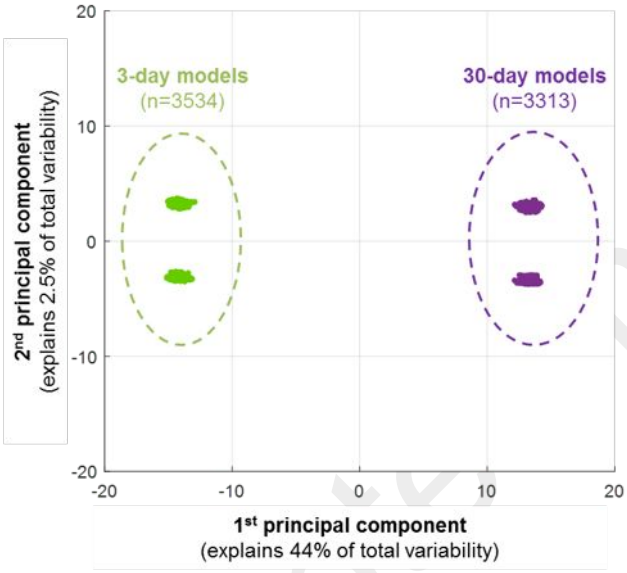

Figure 2. Principal component analysis of 3-day and 30-day subnetworks

We identified reactions that are activated during the differentiation process, by considering the reactions predicted to be inactive in all d3 cell-specific networks but active in at least one of the 30-day cell-specific model (*i.e.*, PA or R at d30). Conversely, reactions predicted to be active at d3 but inactive at d30 were identified as inactivated during differentiation (Figure 1B). According to our predictions, 484 reactions were activated and 200 reactions inactivated during HepaRG cell differentiation. These reactions were further analyzed through pathway enrichment. Activated

reactions were significantly over-represented in known hepato-specific pathways (bile acid synthesis and cytochrome metabolism) but also in the following pathways: biotin metabolism, FA oxidation and tryptophan metabolism. The biotin metabolism pathway acts as a cycle, where the biotin binds to carboxylase enzymes (biotinylation), enabling their activation. Biotin is then released by hydrolysis, to be recycled and re-used for coenzyme activity. Carboxylase enzymes activated by biotinylation are involved in many important cellular functions, related in particular to the production and breakdown of proteins, fats, and carbohydrates and to urea metabolism [40], which are indeed essential in fully functional hepatic cells. The essential amino acid tryptophan is mainly metabolized in the liver through the kynurenine pathway, which accounts for about 95% of its degradation in normal physiological conditions [41]. The prediction of the activation of this pathway in mature hepatocytes is consistent with the observation of the increased activity of enzymes involved in this pathway during the development in rat liver [42]. Conversely, the activity of the extracellular transport pathway and of the FA synthesis pathway was predicted to be lower in 30-day HepaRG cells (Table 1). Our results therefore suggest a shift in the metabolism of FAs, with a decrease in the FA synthesis and a concomitant increase in FA oxidation in differentiated cells.

Table 1. Predictions of metabolic pathways significantly modulated between d3 and d30

ACTIVATED pathways			INACTIVATED pathways		
Pathways	% pathway reactions	corrected p-value	Pathways	% pathway reactions	corrected p-value
Biotin metabolism	100	$1.31e^{-11}$	Transport, extracellular	9.6	$5.60e^{-31}$
Fatty acid oxidation	15.9	$6.80e^{-07}$	Fatty Acid Synthesis	45.2	$1.30e^{-15}$
Bile acid synthesis	27.9	$5.13e^{-05}$			

Tryptophan metabolism	40.0	$2.44e^{-04}$
Cytochrome metabolism	57.1	$3.76e^{-04}$
Blood group synthesis	30.4	$1.59e^{-03}$
Lysine metabolism	50.0	$1.44e^{-03}$
Limonene & pinene degradation	100	$3.45e^{-02}$

Visualization-based mining strengthens metabolic activity comparisons

Although pathway enrichment analysis offers a first global view of the pathways modulated during the differentiation process, some of these pathways, such as the FA synthesis and oxidation pathways, include a very large number of reactions (126 and 868 reactions, respectively). A deeper examination of the reactions modulated within these pathways was carried out using the MetExplore web server for visualization [38,43]. We observed that FA oxidation reactions predicted to be activated between d3 and d30 were specifically located in the peroxisome, whereas most mitochondrial FA oxidation reactions were predicted to be active at both differentiation stages (Figure 3). Notably, peroxisomal FA oxidation allows the specific degradation of very long-chain FAs ($>C_{20}$) whereas the shortened FAs are further oxidized in the mitochondria [44]. Our results therefore imply that increased peroxisomal FA oxidation induced by drugs or FA overload [45] cannot occur in progenitor cells. Although limited peroxisomal FA oxidation can reduce energy production, it primarily induces the accumulation of toxic very long-chain FA metabolites [46]. Regarding the FA synthesis pathway, the visualization highlighted that reactions predicted to be inactivated between d3 and d30 were more specifically involved in the elongation of the carbon chain, suggesting that the synthesis of long-chain FAs cannot be achieved anymore in fully

differentiated hepatocytes. However, transformation of FAs or acyl-CoA, through desaturation or hydrolysis reactions respectively, can be performed at both stages of development (Figure S6).

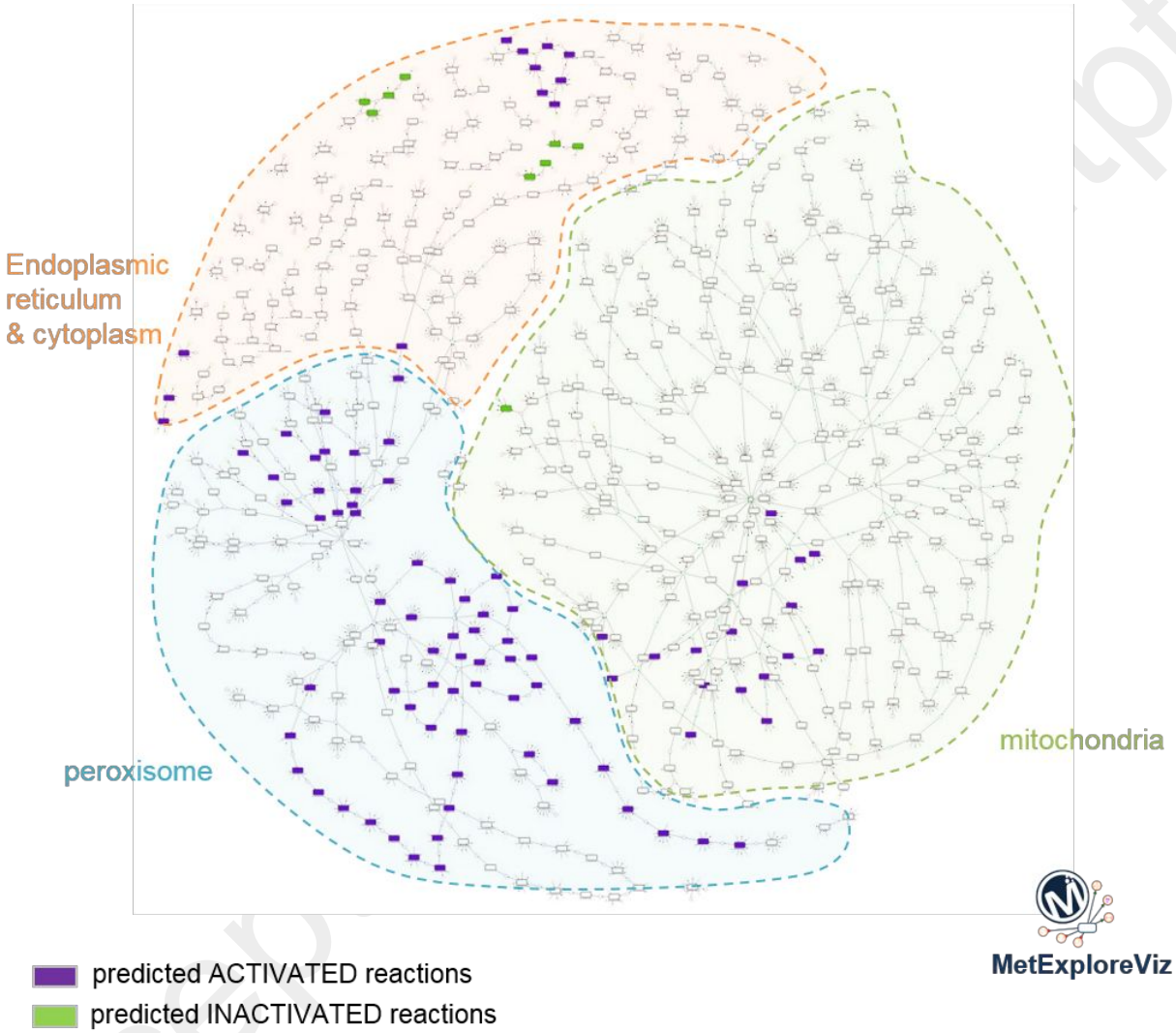

Figure 3. Visualization of predicted modulated reactions in the fatty acid oxidation pathway

Analysis of flux-consistent cell-specific models reveals functional metabolic changes during the differentiation process

To assess whether the generated 3-day and 30-day cell-specific models actually accounted for distinct liver-specific metabolic functionalities, we challenged the capacity of each cell-specific subnetwork to perform 154 defined metabolic functions [4,36,37] (Table S1). Out of this list, 88 functions are generic functions, which can theoretically be achieved by any cell type, and 66 are hepato-specific metabolic functions known to specifically take place in liver, such as ammonia detoxification (through ureagenesis), ketogenesis, biliary acid formation, or gluconeogenesis. On average, a higher number of tested metabolic functions, and especially of liver-specific functions, could be achieved by 30-day cell-specific models compared to 3-day models: 50% *vs.* 31% for hepatic functions and 42% *vs.* 33% for generic functions (Figure 4). Similarly, when comparing the set of all metabolic functions that can be fulfilled by the whole set of models at each stage (*i.e.,* "UNION" of models), we observed that a larger range of hepatic functions can be fulfilled at 30 days than 3 days. More specifically, our models predict that 30-day cells are able to degrade a wider range of amino acids and to produce the ketone body β-hydroxybutyrate compared to 3-day cells (Table 2). Interestingly, this end product of mitochondrial FA oxidation presents different cellular signaling functions in addition to its role in energy production [47]. Regarding the gluconeogenesis capacities, which were assessed by testing the ability of the models to account for the production of glucose in the absence of carbohydrate sources (*e.g.*, from non-carbohydrates metabolites including lactate, pyruvate, glycerol and glucogenic amino acids), results indicate that gluconeogenesis can theoretically be carried out by HepaRG cells at both stages, although by a higher proportion of cell-specific models at d30 than d3. In agreement with the acquisition of liver-specificity over the differentiation process, our models predict that only 30-day cells can produce urea from the degradation of AA (Table 2 & Figure 5) and can synthesize bile acids such as glycocholate, glycochenodeoxycholate and taurocholate.

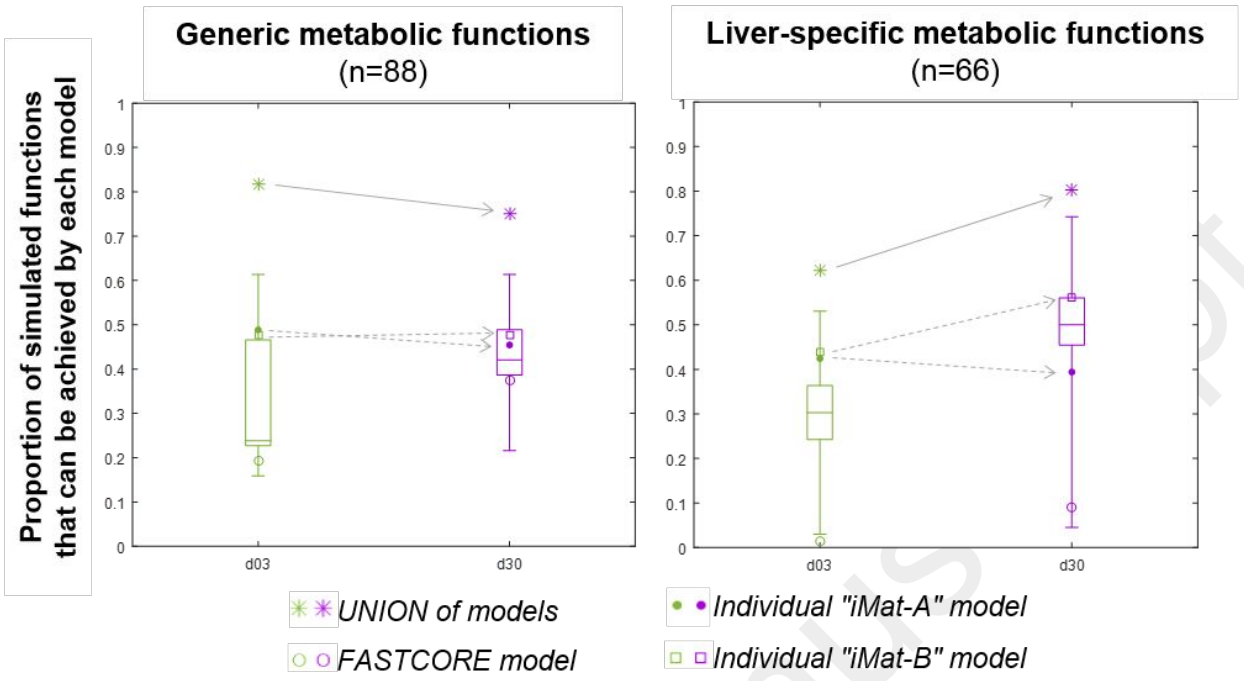

Figure 4. Simulations of metabolic functions in d3 and d30 models.

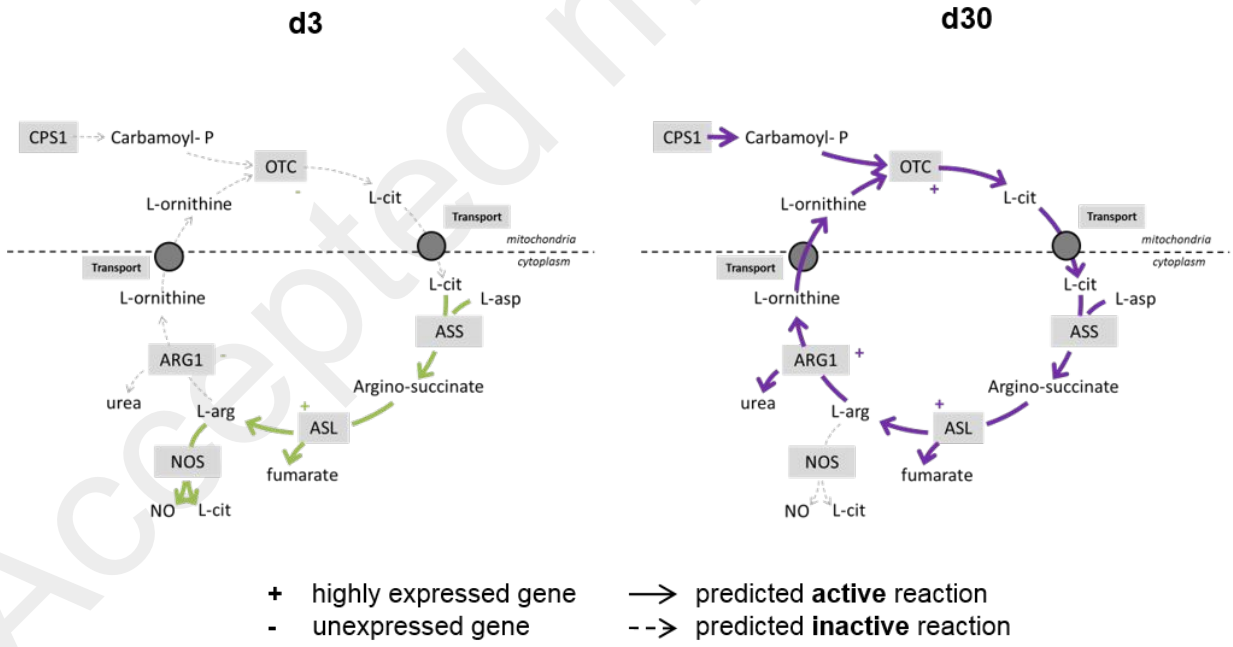

Figure 5. Predicted activities for reactions in the urea cycle

Table 2. Comparison of liver-specific metabolic functionalities between 3-day and 30-day models

	3-day	30-day
Bile acid formation	**1**[a] / 6[b] [0 – 2][c]	**2** / 6 [0 – 6]
Ureogenesis	**0** / 2 [0 – 0]	**2** / 2 [0 – 2]
gluconeogenesis	**4** / 9 [0 – 9]	**6** / 9 [0 – 9]
ketogenesis	**0** / 4 [0 – 2]	**2** / 4 [0 – 4]
Amino acid degradation	**12** / 23 [2 – 17]	**17** / 23 [2 – 23]

We further addressed the ability of progenitor and fully differentiated HepaRG models to account for liver-specificity acquisition, by assessing the proportion (1) of liver-specific genes that were included in each cell-specific subnetwork (based on UNIPROT database annotations, see Material & Methods) and (2) of reactions associated with high confidence level for protein expression in liver (based on the Human Proteome Atlas database information on tissue protein expression, see Material & Methods). We identified that 46% of the Recon 2 genes had evidence for expression in liver. On average, a higher proportion of these liver-expressed genes was recalled in the generated subnetworks representing the 30-day cells (72 to 84% depending on the subnetworks) compared to 3-day cells (64 to 76%), consistent with our expectations (Figure S7). We also obtained a higher recall (and proportion) of reactions expressed in hepatocytes with high confidence level, according to the HPA database, in 30-day HepaRG networks (49 to 53%) compared to 3-day HepaRG networks (36 to 41%) (Figure S8). Globally, these results tend to validate the ability of our developed models to account for the hepatic specialization occurring during cell-differentiation, when considering conjointly all the cell-specific subnetworks identified for each stage.

DISCUSSION

The metabolic status of many *in vitro* models still requires to be duly characterized and this is especially true for models used to study hepatic metabolic diseases, most of which imply, to a certain degree, hepatic regeneration mechanisms. In this study, we propose a methodology, based on large-scale modelling approaches, which enables to point out functional shifts in the global metabolism of cells and apply it to compare the metabolic capacity of hepatic cells at two distinct differentiation stages (progenitor *vs.* fully differentiated cells). Our developed methodology allows gaining a better understanding of metabolic shifts as it can unveil critical information not directly available from experimental data such as gene expression or metabolomics. Transcriptomic data often provide a restricted coverage of the generic metabolic network genes. In our study, gene expression data covered only 31% and 32% of Recon 2 reactions at d3 and d30 respectively when considering the genes present in the initial transcriptomic dataset (Figure S3). The problem related to the partial representation of metabolic network genes with commonly used microarrays is an acknowledged fact, with a coverage that varies depending on the type of microarray used [48]. It should also be noted that the partial coverage of metabolic reactions is partly due to a lack of gene related information for some reactions in the network (35% in Recon 2): these reactions would not be covered whatever the transcriptomic dataset used.. Having such scattered transcriptomic information does not allow to get an overall picture of the metabolic changes occurring during differentiation. By integrating transcriptomic data within the context of a genome-scale metabolic network and computing flux distributions, one takes into account the fact that metabolites used in a reaction need to be produced and consumed, in stoichiometric proportions, by other reactions in the network. Therefore, the activity of a reaction is not only predicted from the expression level of its associated gene but can also be inferred from the activity of downstream and upstream reactions in the network. In our study, 79.2% and 76.5% of the reactions predicted to be active at d3 and d30 (42% of the reactions if solely considering “required” reactions), respectively, were not associated

with any gene expression data and therefore their activity could be newly predicted thanks to the computational method (Figure S9). A large proportion of these reactions belongs to the transport and exchange pathways, which are less well annotated in term of associated genes, but are, nevertheless, key players in cellular and tissue biology and absolutely need to be taken into account to obtain fully flux-consistent networks. Interestingly, the biotin and tryptophan metabolism pathways, for which gene expression data was available for only a small proportion of the reactions (33-53%), could not be predicted as activated on the sole basis of transcriptomic data but their predicted activation was inferred by taking into account the network structure and the connections between reactions (Table S5). On the contrary, a few pathways such as "xenobiotics metabolism", "androgen and estrogen synthesis and metabolism" and "arachidonic acid metabolism" were not predicted as activated, although they would be evidenced as activated if basing solely on gene expression data. This is because most of the reactions in these pathways are blocked reactions (Table S5), meaning that their products cannot be further consumed or their substrates cannot be produced. The Recon 2 network contains almost 30% of "blocked" reactions. Such reactions are always predicted to be inactive when using constraint-based modeling approaches, and can generate false negatives and "artificial" divergences between gene expression data and model predictions that do not have any actual biological meaning. For instance, we observed that 7% (at d3) and 8% (at d30) of the reactions are predicted as inactive although they are associated with HE genes (Figure S9), but 95 to 99% of these reactions are actually blocked reactions, meaning that the observed divergence cannot, in this case, be interpreted as a post-regulation process. More interestingly, when not taking into account blocked reactions, about 1% of the reactions have a predicted activity state that is not in accordance with their associated gene expression data. The discrepancy between data and predictions might also be linked to the presence in the network of promiscuous genes, associated with many different reactions (*e.g.,* the gene EHHADH or hsa:1962

controls 194 reactions). Enforcing a strict translation of the expression or non-expression of such genes to the reaction level would amount to consider that all proteins encoded by a single gene are active (or inactive, respectively) when this gene is expressed (or not/lowly expressed, respectively), which is not biologically relevant. Using the iMat algorithm prevents from doing this strict association, but might consequently generate some discrepancies between predictions and data. In our study, most reactions whose predicted activity is in opposition with their gene expression level belong to extracellular transport and FA oxidation pathways, in which a few genes (respectively 47 and 93) are associated with a large number of reactions (361 and 709 respectively).

Conventional transcriptomic analyses result in lists of identified expressed genes, which are commonly interpreted using pathway enrichment analyses, providing information about which parts of the network are more likely to be differentially expressed in specific experimental conditions [49,50]. However, the definition of metabolic pathways is very dependent on the database or network used and is not always relevant regarding functional metabolism. Indeed, some metabolic functions span over several metabolic pathways, while some metabolic pathways are very generic and encompass several distinct metabolic functions [51]. Thus, one may miss a specific or biologically relevant functionality when relying on these global pathways for interpretation. Generating flux-consistent models of the functional metabolic network of cells offers the clear advantage of going beyond the analysis of metabolic pathways by enabling a more holistically identification of modulated metabolic functions and therefore providing a finer assessment of the metabolic capacities of a system. For instance, in our study, we predicted that ureagenesis is activated during the differentiation process, although the "urea cycle" pathway was not evidenced as activated if relying only on the pathway enrichment analysis (p-value = 1). Indeed, in Recon 2, the "urea cycle pathway" encompasses 69 reactions, but only a few of them are truly involved in urea synthesis (other reactions contribute to creatine or spermidine metabolism) so that the

predicted activation of these reactions was masked by the lack of changes of many other reactions in this pathway.

The originality of the approach we propose in this study mainly relies on the fact that we chose not to arbitrarily select one specific model among all equally optimal cell-specific models identified, but rather to consider them conjointly for each differentiation stage. We observed that the existence of a high number of alternative possible subnetworks is partly due to the existence of redundant reactions in the initial generic reconstruction that often reflect artifactitious redundancies rather than a true biological alternative. Manual curation of these redundancies would contribute to decrease the number of computed equally adequate stage-specific models and therefore reduce the uncertainty in the prediction of reaction activity. Despite this well identified issue, we showed that the comparison of sets of several similarly adequate subnetworks for two distinct conditions still enables evidencing stage-dependent differences, as stage-dependent differences contributed more to the discrimination among all subnetworks than the variability between the subnetworks at each stage (Figure 2). Other methods used to generate cell-specific metabolic models have adopted a different strategy, which consists in selecting one specific solution which optimizes an additional criteria, such as minimizing the total sum of fluxes in the network (Euclidean FBA), maximizing the biomass production or cell growth [52], minimizing the number of active reactions [39] or being able to achieve a set of predefined metabolic tasks [14]. This entails to make some additional and *a priori* assumptions about the "optimal" metabolic state of the cells or some target metabolic functions. This can be relevant in the case of rapidly growing cells, such as cancer cells. However, it is much less relevant for cells that are not in a permanent proliferative status and are able to achieve a wide span of metabolic activities, such as liver cells. We assessed the benefit of our approach by comparing our results with results obtained when considering only one subnetwork for each stage, either arbitrarily selected among all the subnetworks identified by the iMat

algorithm (iMat-A and iMat-B, in Figure 4 & Figures S7 & S8) or generated using the FASTCORE algorithm [39] (see Material and Methods). When considering single solutions, we observed that some metabolic pathways, with little gene expression information, appeared as significantly enriched in activated (*e.g.,* ubiquinone synthesis) or inactivated reactions (*e.g.,* keratan sulfate degradation, N-glycan synthesis) solely as a result of arbitrariness in the choice of the subnetwork at each stage (Table S6), whereas the method developed in this work prevents from making such biased predictions. For instance, the ubiquinone synthesis pathway (Figure S10) was predicted as activated when using the FASTCORE algorithm or considering only one iMat solution. Because no gene-expression information is available at d3 for any of the reactions in this pathway, all these reactions can be predicted to be either active or inactive at d3. As a result and because reactions are necessarily active at d30, whatever the selected subnetwork, it may then be concluded that the pathway is activated if reactions are predicted to be inactive in the retained d3-subnetwork, which is what happens when using the FASTCORE algorithm that aims to minimize the number of reactions (Figure S10C&D). Conversely, with the strategy we implemented in our method, which takes into consideration all the possibilities of reactions activity at d3, we do not predict that this pathway is activated (Figure S10B), retaining a more cautious conclusion. The same interpretations can be made for the N-glycan synthesis and keratin sulfate degradation pathways (Figures S11 & S12 and Supplementary Notes). The FASTCORE algorithm provides one unique minimal subnetwork, which contains all the reactions associated with highly expressed genes and a minimal set of additional reactions required in order to get a flux-consistent network. Although it might reduce the bias in the comparison of the conditions by providing a deterministic way to define one unique model for each condition, we suspect that these minimal networks are more dependent on the transcriptomic data and are likely biased toward assuming that reactions are not active when they have no associated expression data. In addition, it is questionable whether the metabolic state

involving a minimal number of biochemical reactions as computed by the FASTCORE algorithm is truly a good picture of the actual metabolic capacity of a mammalian cell. We reached the conclusion that, in the case of insufficient experimental data, arbitrarily selecting one possible subnetwork could lead to erroneous conclusions and we argue that our method, which takes into account and compares sets of equally optimal subnetworks, prevents from making potentially false positive, and therefore erroneous, predictions regarding the activation or inactivation of pathways.

Getting different results when using different algorithms for identifying cell-specific models is a well acknowledged issue, which has already been reported in several studies [53,54]. No method provides more accurate or exact results than others, and the choice of the method should be made depending on the available experimental data, as well as the context and the aim of the study. However, the approach that we propose here has the advantage not to require any other information than transcriptomic data and does not make any biological assumption about the metabolic state or objective of the cell system. For this reason, it can interestingly be applied to poorly characterized cell systems. Such approaches are nowadays absolutely relevant and necessary for a sound and untargeted assessment of metabolic modulations because they allow for an accurate modeling of cellular metabolic networks out of omics data with a minimal number of *a priori* assumptions and therefore limit the risk of false-predictions. Also, considering all adequately possible subnetworks seem relevant under the hypothesis that the variability observed between the distinct possible subnetworks partly reflects the actual metabolic heterogeneity in a population of cells. Therefore, taking into consideration this variability should provide a better picture of the whole metabolic capability of heterogeneous cellular systems.

CONCLUSION

In conclusion, by implementing a new strategy integrating transcriptomic and metabolomic data within the context of the global human genome-scale metabolic model, we were able to better characterize the metabolic state of HepaRG cells at two stages of differentiation and to identify some metabolic functions that are set up during the differentiation process of this human hepatic model. Our predictions are consistent with the known activation of pathways corresponding to hepato-specific functionalities (bile acid synthesis, cytochrome metabolism) during the differentiation process, but also newly evidenced the modulation of other metabolic pathways, involving the metabolism of biotin, tryptophan and FAs, which could not have been evidenced solely from transcriptomic data. The approach we applied in this study offers several advantages compared to both analyses based on transcriptomic data and common computational approaches used to identify cell- or tissue-specific metabolic models: it especially allows to point out metabolic pathways which do not have gene annotations, to go further the analysis of traditionally defined metabolic pathways by identifying modulated metabolic functions, and to reduce the risk of false predictions by retaining a set of networks instead of a particular (sometime arbitrarily defined) one. The result is that it allows a comprehensive and functional assessment of the metabolic capacity of cells with a minimal number of a priori assumptions. It opens interesting potential for the comparison of global metabolic shifts occurring during differentiation process of various cell types, but also in the broader context of long-term metabolic changes, such as induced during the onset of chronic metabolic diseases or chronic exposure to toxics.

FIGURES

Figure 1. Predicted activity of Recon 2 reactions in stage-specific subnetworks. (A) The activity of Recon 2 reactions was predicted using the iMat algorithm. Several solutions were found and the reactions were classified as "required" (R) if they were found to be active in all solutions and conversely "Inactive" (I) if they display a zero-flux in all the optimal solutions. All other reactions, found to be either active or inactive in the optimal solutions, were classified as "Potentially active" (PA). This analysis was made independently for the d3 and d30 differentiation stages. (B) Reactions identified as I at d3 but R or PA at d30 were considered as activated, whereas reactions identified as R or PA at d3 but I at d30 were considered as activated.

Figure 2. Principal component analysis of 3-day and 30-day subnetworks. PCA analysis was performed on the whole set of equally adequate subnetworks obtained for both stages (n=6847). Reactions were used as variables. Each subnetwork was represented as a binary vector with 0 values for inactive reactions and 1 values for active reactions.

Figure 3. Visualization of predicted modulated reactions in the fatty acid oxidation pathway. Reactions belonging to the fatty acid oxidation pathway in Recon 2 were extracted and visualized using the MetExplore webserver (Chazalviel *et al.*, 2018). Reactions predicted to be activated or inactivated between the 2 differentiation stages were mapped onto the pathway.

Figure 4. Simulations of metabolic functions in 3-day and 30-day models. Metabolic functions were simulated for each of the cell-specific models identified at each stage and for the model obtained using the FASTCORE algorithm. Boxplots represent the distribution of the proportion of simulated functions that can be achieved by 3-day and 30-day cell specific models for all generic (left panel) or all liver-specific (right panel) metabolic functions. UNION of cell-specific models,

represented by a star, corresponds to the proportion of functions that can be achieved by at least one of the cell-specific model. The iMat-A and iMat-B points correspond to the proportion of functions that can be achieved by these 2 randomly selected subnetworks individually. Arrows represent the sense of variation between d3 and d30, which can be different depending on which subnetworks we compare.

Figure 5. Predicted activities for reactions in the urea cycle. Reactions predicted to be active are represented with green plain arrows for d3 and purple plain arrows for d30. "+" and "–" signs indicate reactions associated with highly or unexpressed genes. The following reactions belonging to the urea cycle are represented (names in italic correspond to the reaction identifiers in Recon2): CPS1, carbamoyl-phosphate synthase (*CBPSam & r0034*); OTC, ornithine carbamoyltransferase *(OCBTm);* ASS, argininosuccinate synthase (*ARGSS*); ASL, argininosuccinate lyase (*ARGSL*); ARG1, arginase (*ARGN*); NOS, L-Arginine,NADPH:oxygen oxidoreductase (NO-forming) (*r0145*); ornithine mitochondrial transport exchange with citruline (ORNt4m) (grey circle).

TABLES

Table 1. Predictions of metabolic pathways significantly modulated between d3 and d30

ACTIVATED pathways	
Pathways	corrected p-value
Biotin metabolism	$1.31e^{-11}$
Fatty acid oxidation	$6.80e^{-07}$
Bile acid synthesis	$5.13e^{-05}$
Tryptophan metabolism	$2.44e^{-04}$
Cytochrome metabolism	$3.76e^{-04}$

INACTIVATED pathways	
Pathways	corrected p-value
Transport, extracellular	$5.60e^{-31}$
Fatty Acid Synthesis	$1.30e^{-15}$

Blood group synthesis	$1.59e^{-03}$
Lysine metabolism	$1.44e^{-03}$
Limonene & pinene degradation	$3.45e^{-02}$

Pathway enrichment analysis was performed on set of reactions identified as inactivated (n=200) or activated (n=484) between 3-day and 30-day cell models, after removing blocked reactions. P-values were obtained by performing a hypergeometric test followed by a Bonferroni correction.

Table 2. Comparison of liver-specific metabolic functionalities between 3-day and 30-day models

	d3	**d30**
Bile acid formation	**1**[a] / 6[b] [0 – 2][c]	**2** / 6 [0 – 6]
Ureogenesis	**0** / 2 [0 – 0]	**2** / 2 [0 – 2]
gluconeogenesis	**4** / 9 [0 – 9]	**6** / 9 [0 – 9]
ketogenesis	**0** / 4 [0 – 2]	**2** / 4 [0 – 4]
Amino acid degradation	**12** / 23 [2 – 17]	**17** / 23 [2 – 23]

Results from liver-specific metabolic functions simulated for each of the cell-specific models identified at each stage: for each type of function, values in bold (a) indicate the average number of simulated functions that can be achieved out of the total number of tested functions (b). Values in square brackets (c) correspond to the minimal and maximal numbers of simulated functions that can be achieved.

ASSOCIATED CONTENT

Supporting information.

Principle of the iMat algorithm illustrated on a Toy model (Figure S1); Workflow of analyses implemented for comparison of stage-specific subnetworks (Figure S2); Distribution of genes expression levels in experimental data set and Recon 2 network (Figure S3); Comparison of predicted active reactions in subnetworks between the 2 stages (Figure S4); Analysis of heterogeneity in 30-day subnetworks (Figure S5); Visualization of predicted modulated reactions

in the fatty acid synthesis pathway (Figure S6); Assessment of the liver-specificity of generated subnetworks: comparison with UNIPROT data (Figure S7); Assessment of the liver-specificity of generated subnetworks: comparison with Human Proteome Atlas data (Figure S8); Comparison of predicted reaction activity with gene expression data (Figure S9); Comparison between predictions made from conjoint or individual analysis of cell-specific models for the ubiquinone synthesis pathway (Figure S10); Comparison between predictions made from conjoint or individual analysis of cell-specific models for the N-glycan synthesis pathway (Figure S11); Comparison between predictions made from conjoint or individual analysis of cell-specific models for the keratin sulfate degradation pathway (Figure S12); Adequacy of model predictions with gene expression data (Table S3); Modulated pathways identified using pathway enrichment: comparison between predictions made from generated models & transcriptomic data (Table S5); Modulated pathways identified using pathway enrichment: comparison between predictions made from conjoint or individual analysis of cell-specific models (Table S6). Interpretations of activated or inactivated reactions depending on the selected optimization solution for the Ubiquinone, N-glycan synthesis and keratin sulfate degradation pathways (Supplementary Notes) (PDF)

Metabolic functions used for simulations (Table S1, XLSX)

NMR identified metabolites for 3-day and 30-day HepaRG cells (Table S2, XLSX)

Computed subnetworks for 3-day and 30-day HepaRG cells from our method and the FASTCORE algorithm (Table S4, XLSX)

This material is available free of charge via the Internet at http://pubs.acs.org.

AUTHOR INFORMATION

Present adress

† SRSMC, UMR 7585, Université de Lorraine, France. ‡INSB Institut des sciences biologiques, UMR8204 Centre d'infection et d'immunité de Lille, France.

Author contributions

FJ, NP, AC, FMo and MAR designed the research; FMo, HDS, CC, SB, EP and NC performed the experiments; NP developed the method and performed the computational analysis; FMa, CF and FV participated in the computational analysis; NP wrote the manuscript; FJ, DZ, BF, NC, AC and NP contributed in data interpretation, discussion on results and writing and revising the manuscript.

Funding source

This work was supported by the French Ministry of Research and National Research Agency as part of the French MetaboHUB, the national metabolomics and fluxomics infrastructure (Grant ANR-INBS-0010) and the NISTEC project (Grant ANR-09-CESA-003).

ACKNOWLEDGMENT

This work was supported in part by the French Ministry of Research and the National Research Agency, as part of the French MetaboHUB infrastructure (the national metabolomics and fluxomics infrastructure, Grant ANR-INBS-0010) and the NISTEC project (Grant ANR-09-CESA-003). The authors thank Maxime Chazalviel for its work on metabolic network visualization and Dr Marc Audebert for providing valuable help on experimental procedures.

REFERENCES

(1) Thiele, I.; Palsson, B. Ø. Reconstruction Annotation Jamborees: A Community Approach to Systems Biology. *Mol. Syst. Biol.* **2010**, *6*, 361.

(2) Duarte, N. C.; Becker, S. A.; Jamshidi, N.; Thiele, I.; Mo, M. L.; Vo, T. D.; Srivas, R.; Palsson, B. Ø. Global Reconstruction of the Human Metabolic Network Based on Genomic and Bibliomic Data. *Proc. Natl. Acad. Sci. U. S. A.* **2007**, *104* (6), 1777–1782.

(3) Ma, H.; Sorokin, A.; Mazein, A.; Selkov, A.; Selkov, E.; Demin, O.; Goryanin, I. The Edinburgh Human Metabolic Network Reconstruction and Its Functional Analysis. *Mol Syst Biol* **2007**, *3*, 135.

(4) Mardinoglu, A.; Agren, R.; Kampf, C.; Asplund, A.; Uhlen, M.; Nielsen, J. Genome-Scale Metabolic Modelling of Hepatocytes Reveals Serine Deficiency in Patients with Non-Alcoholic Fatty Liver Disease. *Nat Commun* **2014**, *5* (May 2013), 3083.

(5) Thiele, I.; Swainston, N.; Fleming, R. M. T.; Hoppe, A.; Sahoo, S.; Aurich, M. K.; Haraldsdottir, H.; Mo, M. L.; Rolfsson, O.; Stobbe, M. D.; et al. A Community-Driven Global Reconstruction of Human Metabolism. *Nat Biotechnol* **2013**, *31* (5), 419–425.

(6) Smallbone, K. Striking a Balance with Recon 2.1. **2013**.

(7) Swainston, N.; Smallbone, K.; Hefzi, H.; Dobson, P. D.; Brewer, J.; Hanscho, M.; Zielinski, D. C.; Ang, K. S.; Gardiner, N. J.; Gutierrez, J. M.; et al. Recon 2.2: From Reconstruction to Model of Human Metabolism. *Metabolomics* **2016**, *12* (7), 109.

(8) Blais, E. M.; Rawls, K. D.; Dougherty, B. V; Li, Z. I.; Kolling, G. L.; Ye, P.; Wallqvist, A.;

Papin, J. A. Reconciled Rat and Human Metabolic Networks for Comparative Toxicogenomics and Biomarker Predictions. *Nat. Commun.* **2017**, *8*, 14250.

(9) Brunk, E.; Sahoo, S.; Zielinski, D. C.; Altunkaya, A.; Dräger, A.; Mih, N.; Gatto, F.; Nilsson, A.; Preciat Gonzalez, G. A.; Aurich, M. K.; et al. Recon3D Enables a Three-Dimensional View of Gene Variation in Human Metabolism. *Nat. Biotechnol.* **2018**, *36* (3), 272–281.

(10) Shlomi, T.; Cabili, M. N.; Herrgard, M. J.; Palsson, B. Ø. O.; Ruppin, E.; Herrgård, M. J.; Palsson, B. Ø. O.; Ruppin, E. Network-Based Prediction of Human Tissue-Specific Metabolism. *Nat Biotech* **2008**, *26* (9), 1003–1010.

(11) Jerby, L.; Shlomi, T.; Ruppin, E. Computational Reconstruction of Tissue-Specific Metabolic Models: Application to Human Liver Metabolism. *Mol Syst Biol* **2010**, *6*, 401.

(12) Bordbar, A.; Jamshidi, N.; Palsson, B. O. IAB-RBC-283: A Proteomically Derived Knowledge-Base of Erythrocyte Metabolism That Can Be Used to Simulate Its Physiological and Patho-Physiological States. *BMC Syst Biol* **2011**, *5*, 110.

(13) Agren, R.; Bordel, S.; Mardinoglu, A.; Pornputtapong, N.; Nookaew, I.; Nielsen, J. Reconstruction of Genome-Scale Active Metabolic Networks for 69 Human Cell Types and 16 Cancer Types Using INIT. *PLoS Comput Biol* **2012**, *8* (5), e1002518.

(14) Agren, R.; Mardinoglu, A.; Asplund, A.; Kampf, C.; Uhlen, M.; Nielsen, J. Identification of Anticancer Drugs for Hepatocellular Carcinoma through Personalized Genome-Scale Metabolic Modeling. *Mol. Syst. Biol.* **2014**, *10*, 1–13.

(15) Frezza, C.; Zheng, L.; Folger, O.; Rajagopalan, K. N.; MacKenzie, E. D.; Jerby, L.; Micaroni, M.; Chaneton, B.; Adam, J.; Hedley, A.; et al. Haem Oxygenase Is Synthetically

Lethal with the Tumour Suppressor Fumarate Hydratase. *Nature* **2011**, *477* (7363), 225–228.

(16) Goldstein, I.; Yizhak, K.; Madar, S.; Goldfinger, N.; Ruppin, E.; Rotter, V. P53 Promotes the Expression of Gluconeogenesis-Related Genes and Enhances Hepatic Glucose Production. *Cancer Metab.* **2013**, *1* (1), 9.

(17) Yizhak, K.; Le Dévédec, S. E.; Rogkoti, V. M.; Baenke, F.; de Boer, V. C.; Frezza, C.; Schulze, A.; van de Water, B.; Ruppin, E. A Computational Study of the Warburg Effect Identifies Metabolic Targets Inhibiting Cancer Migration. *Mol. Syst. Biol.* **2014**, *10*, 744.

(18) Orth, J. D.; Thiele, I.; Palsson, B. Ø. O. What Is Flux Balance Analysis? *Nat Biotechnol* **2010**, *28* (3), 245–248.

(19) Zur, H.; Ruppin, E.; Shlomi, T. IMAT: An Integrative Metabolic Analysis Tool. *Bioinformatics* **2010**, *26* (24), 3140–3142.

(20) Aninat, C.; Piton, A.; Glaise, D.; Le Charpentier, T.; Langouët, S.; Morel, F.; Guguen-Guillouzo, C.; Guillouzo, A. Expression of Cytochrome P450 Enzymes and Nuclear Receptors in Human Hepatoma HepaRG Cells. *Drug Metab. Dispos.* **2006**, *34* (1), 75–83.

(21) Rodrigues, R. M.; Heymans, A.; De Boe, V.; Sachinidis, A.; Chaudhari, U.; Govaere, O.; Roskams, T.; Vanhaecke, T.; Rogiers, V.; De Kock, J. Toxicogenomics-Based Prediction of Acetaminophen-Induced Liver Injury Using Human Hepatic Cell Systems. *Toxicol. Lett.* **2016**, *240* (1), 50–59.

(22) Peyta, L.; Jarnouen, K.; Pinault, M.; Guimaraes, C.; Pais de Barros, J.-P.; Chevalier, S.; Dumas, J.-F.; Maillot, F.; Hatch, G. M.; Loyer, P.; et al. Reduced Cardiolipin Content

Decreases Respiratory Chain Capacities and Increases ATP Synthesis Yield in the Human HepaRG Cells. *Biochim. Biophys. Acta - Bioenerg.* **2016**, *1857* (4), 443–453.

(23) Ma, X.; Duan, Y.; Tschudy-Seney, B.; Roll, G.; Behbahan, I. S.; Ahuja, T. P.; Tolstikov, V.; Wang, C.; McGee, J.; Khoobyari, S.; et al. Highly Efficient Differentiation of Functional Hepatocytes From Human Induced Pluripotent Stem Cells. *Stem Cells Transl. Med.* **2013**, *2* (6), 409–419.

(24) Zhang, J.; Nuebel, E.; Daley, G. Q.; Koehler, C. M.; Teitell, M. A. Metabolic Regulation in Pluripotent Stem Cells during Reprogramming and Self-Renewal. *Cell Stem Cell* **2012**, *11* (5), 589–595.

(25) Xu, X.; Duan, S.; Yi, F.; Ocampo, A.; Liu, G.-H.; Izpisua Belmonte, J. C. Mitochondrial Regulation in Pluripotent Stem Cells. *Cell Metab.* **2013**, *18* (3), 325–332.

(26) Teslaa, T.; Teitell, M. A. Pluripotent Stem Cell Energy Metabolism: An Update. *EMBO J.* **2015**, *34* (2), 138–153.

(27) Bucher, S.; Jalili, P.; Le Guillou, D.; Begriche, K.; Rondel, K.; Martinais, S.; Zalko, D.; Corlu, A.; Robin, M.-A.; Fromenty, B. Bisphenol a Induces Steatosis in HepaRG Cells Using a Model of Perinatal Exposure. *Environ. Toxicol.* **2017**, *32* (3), 1024–1036.

(28) Cerec, V.; Glaise, D.; Garnier, D.; Morosan, S.; Turlin, B.; Drenou, B.; Gripon, P.; Kremsdorf, D.; Guguen-Guillouzo, C.; Corlu, A. Transdifferentiation of Hepatocyte-like Cells from the Human Hepatoma HepaRG Cell Line through Bipotent Progenitor. *Hepatology* **2007**, *45*, 957–967.

(29) Hart, S. N.; Li, Y.; Nakamoto, K.; Subileau, E. a.; Steen, D.; Zhong, X. b. A Comparison of

Whole Genome Gene Expression Profiles of HepaRG Cells and HepG2 Cells to Primary Human Hepatocytes and Human Liver Tissues. *Drug Metab. Dispos.* **2010**, *38* (6), 988–994.

(30) Parent, R.; Beretta, L. Translational Control Plays a Prominent Role in the Hepatocytic Differentiation of HepaRG Liver Progenitor Cells. *Genome Biol.* **2008**, *9*, R19.

(31) Wishart, D. S.; Jewison, T.; Guo, A. C.; Wilson, M.; Knox, C.; Liu, Y.; Djoumbou, Y.; Mandal, R.; Aziat, F.; Dong, E.; et al. HMDB 3.0—The Human Metabolome Database in 2013. *Nucleic Acids Res.* **2012**, *41* (D1), D801–D807.

(32) Rossell, S.; Huynen, M. A.; Notebaart, R. A. Inferring Metabolic States in Uncharacterized Environments Using Gene-Expression Measurements. *PLoS Comput Biol* **2013**, *9* (3), e1002988.

(33) UniProt: The Universal Protein Knowledgebase. *Nucleic Acids Res.* **2017**, *45* (D1), D158–D169.

(34) Uhlen, M.; Fagerberg, L.; Hallstrom, B. M.; Lindskog, C.; Oksvold, P.; Mardinoglu, A.; Sivertsson, A.; Kampf, C.; Sjostedt, E.; Asplund, A.; et al. Tissue-Based Map of the Human Proteome. *Science (80-.).* **2015**, *347* (6220), 1260419–1260419.

(35) Dennis, G.; Sherman, B. T.; Hosack, D. A.; Yang, J.; Gao, W.; Lane, H.; Lempicki, R. A.; Quackenbush, J.; Wheeler, D.; Chappey, C.; et al. DAVID: Database for Annotation, Visualization, and Integrated Discovery. *Genome Biol.* **2003**, *4* (9), R60.

(36) Bordbar, A.; Feist, A. M.; Usaite-Black, R.; Woodcock, J.; Palsson, B. O.; Famili, I. A Multi-Tissue Type Genome-Scale Metabolic Network for Analysis of Whole-Body Systems Physiology. *BMC Syst Biol* **2011**, *5*, 180.

(37) Gille, C.; Bolling, C.; Hoppe, A.; Bulik, S.; Hoffmann, S.; Hubner, K.; Karlstadt, A.; Ganeshan, R.; Konig, M.; Rother, K.; et al. HepatoNet1: A Comprehensive Metabolic Reconstruction of the Human Hepatocyte for the Analysis of Liver Physiology. *Mol Syst Biol* **2010**, *6* (411), 411.

(38) Cottret, L.; Wildridge, D.; Vinson, F.; Barrett, M. P.; Charles, H.; Sagot, M. F.; Jourdan, F. MetExplore: A Web Server to Link Metabolomic Experiments and Genome-Scale Metabolic Networks. *Nucleic Acids Res* **2010**, *38* (Web Server issue), W132-7.

(39) Vlassis, N.; Pacheco, M. P.; Sauter, T. Fast Reconstruction of Compact Context-Specific Metabolic Network Models. *arXiv:1304.7992 [q-bio.MN]* **2013**, *10*, 1–15.

(40) Tong, L. Structure and Function of Biotin-Dependent Carboxylases. *Cell. Mol. Life Sci.* **2013**, *70* (5), 863–891.

(41) Badawy, A. A.-B. Tryptophan Metabolism, Disposition and Utilization in Pregnancy. *Biosci. Rep.* **2015**, *35* (5), e00261–e00261.

(42) Suda, T.; Robinson, J. C.; Fjellstedt, T. A. Developmental Changes in the Enzymatic Capacity for Reduction and Oxidation of Alpha-Ketoadipate in Rat Liver, Heart, Kidney, and Brain. *Pediatr. Res.* **1978**, *12* (4 Pt 1), 297–300.

(43) Chazalviel, M.; Frainay, C.; Poupin, N.; Vinson, F.; Merlet, B.; Gloaguen, Y.; Cottret, L.; Jourdan, F. MetExploreViz: Web Component for Interactive Metabolic Network Visualization. *Bioinformatics* **2018**, *34* (2), 312–313.

(44) Wanders, R. J. A.; Waterham, H. R.; Ferdinandusse, S. Metabolic Interplay between Peroxisomes and Other Subcellular Organelles Including Mitochondria and the

907 Endoplasmic Reticulum. *Front. Cell Dev. Biol.* **2016**, *3*, 83.

908 (45) Kersten, S. Integrated Physiology and Systems Biology of PPARα. *Mol. Metab.* **2014**, *3* (4),
909 354–371.

910 (46) Fan, C. Y.; Pan, J.; Chu, R.; Lee, D.; Kluckman, K. D.; Usuda, N.; Singh, I.; Yeldandi, A.
911 V; Rao, M. S.; Maeda, N.; et al. Hepatocellular and Hepatic Peroxisomal Alterations in Mice
912 with a Disrupted Peroxisomal Fatty Acyl-Coenzyme A Oxidase Gene. *J. Biol. Chem.* **1996**,
913 *271* (40), 24698–24710.

914 (47) Newman, J. C.; Verdin, E. β-Hydroxybutyrate: A Signaling Metabolite. *Annu. Rev. Nutr.*
915 **2017**, *37* (1), 51–76.

916 (48) Zelezniak, A.; Pers, T. H.; Soares, S.; Patti, M. E.; Patil, K. R. Metabolic Network Topology
917 Reveals Transcriptional Regulatory Signatures of Type 2 Diabetes. *PLoS Comput. Biol.*
918 **2010**, *6* (4), e1000729.

919 (49) Chagoyen, M.; Pazos, F. MBRole: Enrichment Analysis of Metabolomic Data.
920 *Bioinformatics* **2011**, *27* (5), 730–731.

921 (50) Persicke, M.; Rückert, C.; Plassmeier, J.; Stutz, L. J.; Kessler, N.; Kalinowski, J.; Goesmann,
922 A.; Neuweger, H. MSEA: Metabolite Set Enrichment Analysis in the MeltDB Metabolomics
923 Software Platform: Metabolic Profiling of Corynebacterium Glutamicum as an Example.
924 *Metabolomics* **2012**, *8* (2), 310–322.

925 (51) Frainay, C.; Jourdan, F. Computational Methods to Identify Metabolic Sub-Networks Based
926 on Metabolomic Profiles. *Brief. Bioinform.* **2017**, *18* (1), 43–56.

927 (52) Becker, S. A.; Palsson, B. O. Context-Specific Metabolic Networks Are Consistent with

Experiments. *PLoS Comput. Biol.* **2008**, *4* (5), e1000082.

(53) Machado, D.; Herrgård, M. Systematic Evaluation of Methods for Integration of Transcriptomic Data into Constraint-Based Models of Metabolism. *PLoS Comput. Biol.* **2014**, *10* (4), e1003580.

(54) Pacheco, M. P.; Pfau, T.; Sauter, T. Benchmarking Procedures for High-Throughput Context Specific Reconstruction Algorithms. *Front. Physiol.* **2016**, *6*, 410.

For Table of Content only